The squirrel-cage induction motor model and its parameter identification via steady and dynamic tests

Onofre A. Morfín[1], Carlos E. Castañeda[2], Riemann Ruiz-Cruz[3], Fredy A. Valenzuela[4],

Miguel A. Murillo[5], Abel E. Quezada[6], and Nahitt Padilla[7]

[1,5,6,7]Universidad Autónoma de Ciudad Juárez, Ciudad Juárez, Chih. México, email: [1]omorfin@uacj.mx,

[5]miguel.murillo@uacj.mx, [6]abquezad@uacj.mx, [7]jpadilla@uacj.mx

[2]Centro Universitario de los Lagos, Unversidad de Guadalajara, e-mail: ccastaneda@lagos.udg.mx

[3]riemannruiz@iteso.mx, [4]fredy.valenzuela@ujat.mx.

One of the most important bases for designing robust closed-loop controllers applied to induction motor with high performance is establishing its mathematical model and state observers, as well as the parameter identification with high accuracy. On this paper, a step-by-step mathematical model of the squirrel-cage induction motor is described at $\alpha\beta$ coordinate frame where the parameters are defined in detailed form; the rotor flux linkages and load torque are estimated via an asymptotic observer; the induction motor parameter identification is performed via a data acquisition board, applying dynamic and steady-state tests. Inductances of the induction motor model are calculated using the proposed relationships between the magnetically-coupled circuit and equivalent circuit model. The mathematical model, state observers and parameter identification procedure of squirrel-cage induction motor are validated via comparison of simulation signals with their corresponding real-time signals. This validation is made experimentally by a steady state test, where load conditions are changed via a dynamometer which is belt coupled with the squirrel-cage induction motor.

1 Introduction

The induction machine is one of the most common electrical motors used today. This motor has many

applications, due that, it is a rugged, highly reliable, low cost and almost maintenance-free electrome-

chanical device. Despite of being a common device, one drawback of this motor is that its mathematical

model is very complex, due to its non-linearity and time variant parameters. The procedure to develop

an induction motor model, and the procedure to identify its parameters is difficult. Several authors have

been addressed modeling and parameter identification, which are very important aspects for designing

control algorithms, but they not present many details. A novel parameter identification process where a single-phase ac test is applied to make the induction motor stand-still is proposed in [1], [2], and [3], diverse ac signals are feeding in only two terminals and no electromagnetic torque is generated. They propose a monophasic equivalent circuit at terminals $a - b$ and apply an input-output test with the prediction error method to obtain indirectly the parameter vector with components: R_s, L_s, σ, and T_r. The work reported in [1] and [2] includes saturation magnetic in both total-leakage inductance and magnetizing inductance. They discretize the standstill-test circuit impedance to apply an input-output test and obtain the parameter vector. In [3] the input and output signals, i.e. voltage and current stator, respectively, are analyzed by the fast Fourier transform algorithm; the analog low-pass filters are used to cut off the harmonics around the switching frequency of these signals. The stator voltage, stator current and their derivatives, necessary for the recursive least squares algorithm, are obtained using the vector constructing method. [1], [2], and [3] do not present the relationships between the inductances values obtained with the ones used in the dynamic model. The parameter identification process results a little complex and the mechanical parameters are not obtained.

The off-line motor parameter identification method applying the no-load and rated-running tests with measurements in the sinusoidal steady-state mode is other technique; this process applies linear regression and estimates the equivalent circuit parameters, [4], [5], and [6]. In [4] a recursive simple least-square algorithm is applied using the real and complex components of the transfer function between voltages and currents by simulations with different noise sources. They apply DC-test for estimating R_s; no-load test for estimating R_f and X_m, and rated-load test for estimating X_l and R. However, the relationships between the inductances from equivalent circuit proposed and the ones of the dynamic model are not clear which makes it difficult to interpret. Moreover, they do not report the mechanical parameters. In [5], this paper deals with off-line parameter identification from input-output data (stator voltages-stator currents and velocity) supplying the motor with steady-state sinusoidal voltages. The parameter identification is made by the standard recursive least squares (RLS) algorithm for minimizing the model prediction error, but they do not consider the rotor leakage inductance and determine only the equivalent circuit parameters. In [6], the authors propose an off-line motor parameter identification method applying model reference adaptive system (MRAS) scheme that uses a global optimization al-

gorithm based on sparse grid method named the hyperbolic cross point (HCP) algorithm. The measured and simulated stator currents are compared in a cost function to define in recursive form the following set of parameters: R_s, R'_r, L_{Ls}, L_s, H, and LL. The authors commit a mistake defining the mutual inductance for dynamical model because they forget the coefficient term of 3/2.

Other parameter identification process is applied from the starting-test results to refer some output variables with respect to slip changes, [7] and [8]. In [7], based on steady-state circuit equivalent, the parameter identification is realized using electric torque and motor current measures, which are taken at different slip values. The parameter estimation is performed off-line using a multi-objective genetic algorithm to minimize the error between the measured data and the data obtained from equivalent circuit. The genetic algorithm represents a high computational load, which makes a complicated implementation. In addition, that research does not present the relationships between the inductances values obtained with the ones used in the dynamic model, and the mechanical parameters are not obtained. In [8] from starting no-load test at low voltage, the resistance and reactance curves are depicted in function of the slip rate, then the recursive least squares (RLS) algorithm combined with a particle swarm optimization method is applied to optimize the equivalent circuit parameters. However, the friction coefficient and inertial moment is calculated via the equation movement from the electromagnetic torque using the rotor resistance whose value is sensitive to temperature changes.

On-line parameter estimation consists of identifying the evolution of the machine parameters without removing the machine from service, [9]-[10]. In [9] a two-step approach to identify the parameters of an induction machine from the measures of the stator currents at starting-test is presented. This proposal uses both simulation and estimation processes; in the first stage, an input-output response of the forward induction motor model with low-quality initial guesses is used to generate a set of predictions of the stator currents $\hat{\mathbf{i}}_s$; then, in the second stage, the input is the mismatch between the estimated and measured stator current vector having as output a parameter vector; this process is made in recursive form applying the Levenberg-Marquardt algorithm until the mismatch of currents is minimized. In [10], a multi-rate real time model-based parameter estimation algorithms for induction motor are applied. The proposed multi-rate EFK method combines multi-rate control and EFK to estimate motor load torque, introducing both input and output algorithms. The method is implemented in real time on a PC cluster

node that acts as a controller to an induction motor experimental set-up. This paper only estimate the rotor time constant and the method represents a high computational load, which makes a complicated implementation.

After having reviewed some research about parametric estimation and modeling of the induction motor, we have identified the importance of establishing, in a detailed and clear way, the procedure for obtaining the model of the induction motor and the identification of all parameters, both electrical and mechanical. Thus, from this base knowledge, innovative identification techniques more accurate can be applied. Therefore, the main contributions of this research are: 1) a detailed procedure to obtain the mathematical model for the squirrel-cage induction motor where the rotor inductance, stator inductance and mutual inductance are defined formally when setting the model at $\alpha\beta$ coordinate frame; this methodology can be applied to obtain the mathematical model of any other type of ac machine, such as the doubly-fed induction generator, synchronous machine, and permanent-magnet machine; 2) the electrical parameter identification is made via a data acquisition board including the electrical variables of all phases and computing the consumed power in each one test with accuracy; in addition, the synchronous test was made to quantify the core loss; 3) for comparison purposes, a complete equivalent circuit including core-loss is proposed with goal of validate the common approaches performed in standstill test and no-load test which define the equivalent circuit model.

This paper is organized as follows. In section 2, the induction motor mathematical model at $\alpha\beta$ frame, rotor flux linkages observer and load torque observer, are developed in detail. The identification procedure for estimating the electrical and mechanical parameters of the induction motor is presented in section 3, where each experiment is explained in detail. In order to validate the mathematical model and its parameter identification, a comparison between simulated and real-time experimental results are discussed in section 4. Finally, the conclusions are given in section 5.

2 The squirrel-cage induction motor model

The voltage vector equations in machine variables for the stator winding and rotor winding, respectively, are:

$$\mathbf{v}_{ABC} = \mathbf{R}_s \mathbf{i}_{ABC} + \frac{d}{dt}\boldsymbol{\lambda}_{ABC} \ , \tag{1}$$

$$\mathbf{v}'_{abc} = \mathbf{R}_r \mathbf{i}'_{abc} + \frac{d}{dt} \boldsymbol{\lambda}'_{abc} \, , \qquad (2)$$

with

$$\mathbf{R}_s = \begin{bmatrix} R_s & 0 & 0 \\ 0 & R_s & 0 \\ 0 & 0 & R_s \end{bmatrix} , \mathbf{R}_r = \begin{bmatrix} R'_r & 0 & 0 \\ 0 & R'_r & 0 \\ 0 & 0 & R'_r \end{bmatrix} .$$

In the above equations capital letter suffixes are used to identify the stator variables and lowercase letters to rotor variables. R_s is the stator resistance per phase, and R'_r is the rotor resistance per phase referred to stator winding. When considering linearity in the flux linkages-current relation ($\lambda - i$), the stator and rotor flux linkages vector equations may be expressed in abc system as:

$$\boldsymbol{\lambda}_{ABC} = \mathbf{L}_s \mathbf{i}_{ABC} + \mathbf{L}_{sr} \mathbf{i}_{abc} \, , \qquad (3)$$

$$\boldsymbol{\lambda}'_{abc} = \mathbf{L}_r \mathbf{i}_{abc} + \mathbf{L}_{sr}^{\top} \mathbf{i}_{ABC} \, , \qquad (4)$$

with

$$\mathbf{L}_s = \begin{bmatrix} L_{ss} & L_{sm} & L_{sm} \\ L_{sm} & L_{ss} & L_{sm} \\ L_{sm} & L_{sm} & L_{ss} \end{bmatrix} ,$$

$$\mathbf{L}_{sr} = L_{srm} \begin{bmatrix} \cos \theta_r & \cos \left(\theta_r + \frac{2\pi}{3}\right) & \cos \left(\theta_r - \frac{2\pi}{3}\right) \\ \cos \left(\theta_r - \frac{2\pi}{3}\right) & \cos \theta_r & \cos \left(\theta_r + \frac{2\pi}{3}\right) \\ \cos \left(\theta_r + \frac{2\pi}{3}\right) & \cos \left(\theta_r - \frac{2\pi}{3}\right) & \cos \theta_r \end{bmatrix} ,$$

$$\mathbf{L}_r = \begin{bmatrix} L'_{rr} & L'_{rm} & L'_{rm} \\ L'_{rm} & L'_{rr} & L'_{rm} \\ L'_{rm} & L'_{rm} & L'_{rr} \end{bmatrix} ,$$

where L_{ss} and L_{sm} are the stator self-inductance per phase and stator mutual-inductance between two phases, respectively; and L_{srm} is the amplitude of the mutual inductances between stator and rotor windings; L'_{rr} and L'_{rm} are the rotor self-inductance per phase and rotor mutual-inductance between two phases, respectively; both are referred to the stator side. It is important to remark that the mutual-inductances between two windings vary periodically due to the relative movement between the stator winding and rotor winding.

In order to remove the time dependency of the mutual-inductances between the stator and rotor windings, the Clarke similitude transformation is applied to change the electrical variables from abc system to $\alpha\beta0$ coordinate

frame, whose axes are fixed on the stator winding and the α-axis is aligned with the phase-a axis [11], see Fig. 1.

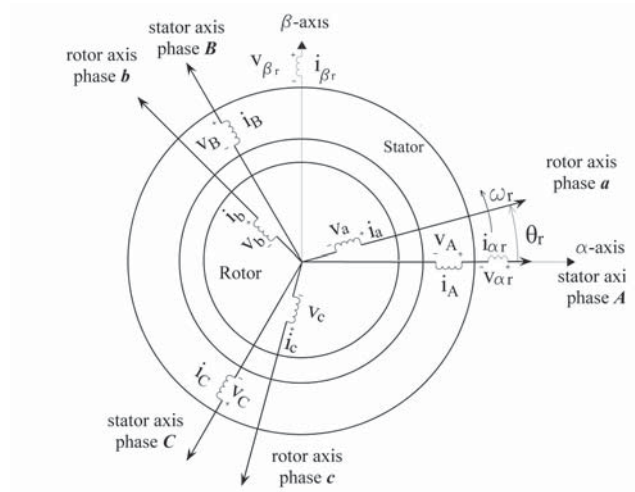The Clarke transformation matrix and its inverse matrix applied to stator variables are defined as:

$$
\mathbf{T}_s = \frac{2}{3}
\begin{bmatrix}
1 & -\frac{1}{2} & -\frac{1}{2} \\
0 & \frac{\sqrt{3}}{2} & -\frac{\sqrt{3}}{2} \\
\frac{\sqrt{2}}{2} & \frac{\sqrt{2}}{2} & \frac{\sqrt{2}}{2}
\end{bmatrix},
\tag{5}
$$

$$
\mathbf{T}_s^{-1} =
\begin{bmatrix}
1 & 0 & \frac{\sqrt{2}}{2} \\
-\frac{1}{2} & \frac{\sqrt{3}}{2} & \frac{\sqrt{2}}{2} \\
-\frac{1}{2} & -\frac{\sqrt{3}}{2} & \frac{\sqrt{2}}{2}
\end{bmatrix}.
\tag{6}
$$

Conducive to transform the rotor variables into new a coordinate system, the displacement angle θ_r must be considered, as it is depicted in Fig. 1. Then, the similitude transformation and its inverse representation applied to rotor variables are defined as:

$$
\mathbf{T}_r = \frac{2}{3}
\begin{bmatrix}
\cos \theta_r & \cos \left(\theta_r + \frac{2\pi}{3}\right) & \cos \left(\theta_r - \frac{2\pi}{3}\right) \\
\sin \theta_r & \sin \left(\theta_r + \frac{2\pi}{3}\right) & \sin \left(\theta_r - \frac{2\pi}{3}\right) \\
\frac{\sqrt{2}}{2} & \frac{\sqrt{2}}{2} & \frac{\sqrt{2}}{2}
\end{bmatrix},
\tag{7}
$$

$$
\mathbf{T}_r^{-1} =
\begin{bmatrix}
\cos \theta_r & \sin \theta_r & \frac{\sqrt{2}}{2} \\
\cos \left(\theta_r + \frac{2\pi}{3}\right) & \sin \left(\theta_r + \frac{2\pi}{3}\right) & \frac{\sqrt{2}}{2} \\
\cos \left(\theta_r - \frac{2\pi}{3}\right) & \sin \left(\theta_r - \frac{2\pi}{3}\right) & \frac{\sqrt{2}}{2}
\end{bmatrix}.
\tag{8}
$$

Figure 1. Clarke transformation applied to stator and rotor variables.

By applying the Clarke transformation (5)-(6) to stator voltage equation (1) gives the next result:

$$\mathbf{v}_{\alpha\beta 0s} = \mathbf{R}_s \mathbf{i}_{\alpha\beta 0s} + \frac{d}{dt}\boldsymbol{\lambda}_{\alpha\beta 0s}, \tag{9}$$

with

$$\mathbf{R}_s = \begin{bmatrix} R_s & 0 & 0 \\ 0 & R_s & 0 \\ 0 & 0 & R_s \end{bmatrix}.$$

Meanwhile, the stator flux linkages vector in $\alpha\beta 0$ takes the following form, when the similitude transformations (5)-(6) and (7)-(8) are applied into (3):

$$\boldsymbol{\lambda}_{\alpha\beta 0s} = \mathbf{L}_s \mathbf{i}_{\alpha\beta 0s} + \mathbf{L}_{sr} \mathbf{i}_{\alpha\beta 0r}, \tag{10}$$

with

$$\mathbf{L}_s = \begin{bmatrix} L_s & 0 & 0 \\ 0 & L_s & 0 \\ 0 & 0 & L_{ss} + 2L_{sm} \end{bmatrix}, \mathbf{L}_{sr} = \begin{bmatrix} L_m & 0 & 0 \\ 0 & L_m & 0 \\ 0 & 0 & 0 \end{bmatrix}$$

where the stator-inductance and mutual-inductance are defined, respectively, as:

$$L_s = L_{ss} - L_{sm}, \tag{11}$$

and

$$L_m = \frac{3}{2}L_{srm}. \tag{12}$$

By applying the similitude transformation (7)-(8) into (2), the rotor voltage vector in $\alpha\beta 0$ frame becomes:

$$\mathbf{v}_{\alpha\beta 0r} = \mathbf{R}_r \mathbf{i}_{\alpha\beta 0r} + \boldsymbol{\Omega}_r \boldsymbol{\lambda}_{\alpha\beta 0r} + \frac{d}{dt}\boldsymbol{\lambda}_{\alpha\beta 0r}, \tag{13}$$

where

$$\mathbf{R}_r = \begin{bmatrix} R'_r & 0 & 0 \\ 0 & R'_r & 0 \\ 0 & 0 & R'_r \end{bmatrix}, \boldsymbol{\Omega}_r = \begin{bmatrix} 0 & \omega_r & 0 \\ -\omega_r & 0 & 0 \\ 0 & 0 & 0 \end{bmatrix}$$

with $\omega_r = \frac{P}{2}\omega_m$ as the rotor frequency, P is the number of poles and ω_m is the rotor angular velocity.

Using the similitude transformations (5)-(6) and (7)-(8) into the rotor flux linkages vector (4), results:

$$\boldsymbol{\lambda}_{\alpha\beta 0r} = \mathbf{L}_r \mathbf{i}_{\alpha\beta 0r} + \mathbf{L}_{sr} \mathbf{i}_{\alpha\beta 0s}, \tag{14}$$

with

$$\mathbf{L}_r = \begin{bmatrix} L_r & 0 & 0 \\ 0 & L_r & 0 \\ 0 & 0 & L_{rr} + 2L_{rm} \end{bmatrix}, \mathbf{L}_{sr} = \begin{bmatrix} L_m & 0 & 0 \\ 0 & L_m & 0 \\ 0 & 0 & 0 \end{bmatrix}$$

where the rotor-inductance is defined as:

$$L_r = L_{rr} - L_{rm} \ . \tag{15}$$

The simplest representation of the induction motor model uses the stator current vector is $\mathbf{i}_s$ and rotor flux linkages vector $\boldsymbol{\lambda}_r$ as state variables, and its order is reduced using only components in α and β axes, since the variables at 0 axis are not present due to the neutral connection at stator winding is not grounded. By solving for $\mathbf{i}_r$ into rotor flux linkages vector (14), we obtain:

$$\mathbf{i}_r = \mathbf{L}_r^{-1} \left(\boldsymbol{\lambda}_r - \mathbf{L}_{sr} \mathbf{i}_s \right) \ . \tag{16}$$

Substituting equation (16) in the rotor voltage equation (13), defining $\mathbf{v}_r = 0$ due to the conducting bars are shorted at both ends via rings in the rotor's squirrel-cage, and solving $\dfrac{d}{dt} \boldsymbol{\lambda}_r$ in equation (13), we obtain the state equation of rotor flux linkages vector in $\alpha\beta$ frame as follows:

$$\frac{d}{dt} \begin{bmatrix} \lambda_{\alpha r} \\ \lambda_{\beta r} \end{bmatrix} = \begin{bmatrix} -\frac{1}{T_r} & -\frac{P}{2}\omega_m \\ \frac{P}{2}\omega_m & -\frac{1}{T_r} \end{bmatrix} \begin{bmatrix} \lambda_{\alpha r} \\ \lambda_{\beta r} \end{bmatrix} + \begin{bmatrix} \frac{L_m}{T_r} & 0 \\ 0 & \frac{L_m}{T_r} \end{bmatrix} \begin{bmatrix} i_{\alpha s} \\ i_{\beta s} \end{bmatrix} \ . \tag{17}$$

Now, substituting the stator flux linkage equation (10) into the stator voltage equation (9), results in:

$$\mathbf{v}_s = \mathbf{R}_s \mathbf{i}_s + \mathbf{L}_s \frac{d}{dt} \mathbf{i}_s + \mathbf{L}_{sr} \frac{d}{dt} \mathbf{i}_r \ . \tag{18}$$

Substituting the differentiation of the rotor current vector (16) into equation (18), and solving for the term $\dfrac{d}{dt} \mathbf{i}_s$, we obtain the state equations of stator current vector in $\alpha\beta$ frame as follows:

$$\frac{d}{dt} \begin{bmatrix} i_{\alpha s} \\ i_{\beta s} \end{bmatrix} = \begin{bmatrix} \frac{\delta}{T_r} & \frac{P}{2}\delta\omega_m \\ -\frac{P}{2}\delta\omega_m & \frac{\delta}{T_r} \end{bmatrix} \begin{bmatrix} \lambda_{\alpha r} \\ \lambda_{\beta r} \end{bmatrix} + \begin{bmatrix} -\gamma & 0 \\ 0 & -\gamma \end{bmatrix} \begin{bmatrix} i_{\alpha s} \\ i_{\beta s} \end{bmatrix} + \begin{bmatrix} \frac{1}{\sigma L_s} & 0 \\ 0 & \frac{1}{\sigma L_s} \end{bmatrix} \begin{bmatrix} v_{\alpha s} \\ v_{\beta s} \end{bmatrix} \tag{19}$$

On the other hand, the electromagnetic torque developed by induction motor, as a torsional force, is defined by the variation of stored magnetic field energy with respect to electric angular position as:

$$T_e = \left(\frac{P}{2} \right) \frac{dW_f}{d\theta_r} \ , \tag{20}$$

where P is the poles number of machine, and the stored field energy is defined by [11], [12]:

$$
W_f = \frac{1}{2} \left(\mathbf{i}_{ABC} \right)^\top \mathbf{L}_{ss} \mathbf{i}_{ABC} + \left(\mathbf{i}_{ABC} \right)^\top \mathbf{L}_{sr} \mathbf{i}_{abcr}
$$
$$
+ \frac{1}{2} \left(\mathbf{i}_{abc} \right)^\top \mathbf{L}_{rr} \mathbf{i}_{abc}. \tag{21}
$$

Because $\mathbf{L}_{ss}$ and $\mathbf{L}_{rr}$ are not functions of θ_r, substituting the stored field energy (21) into (20), yields the electromagnetic torque in abc system:

$$
T_e = \left(\frac{P}{2} \right) \frac{\partial}{\partial \theta_r} \left[\left(\mathbf{i}_{ABC} \right)^\top \mathbf{L}_{sr} \mathbf{i}_{abc} \right] . \tag{22}
$$

Applying the similitude transformations (5)-(6) and (7)-(8) to stator current and rotor currents, respectively in (22); and substituting the mutual-inductance L_m defined in (12), the electromagnetic torque in terms of $\alpha\beta$ coordinate frame takes the form:

$$
T_e = \left(\frac{3}{2} \right) \left(\frac{P}{2} \right) L_m \mathbf{i}_s^\top \begin{bmatrix} 0 & 1 \\ -1 & 0 \end{bmatrix} \mathbf{i}_r , \tag{23}
$$

Now, substituting the rotor current equation (16) into (23), the electromagnetic torque, expressed with the rotor flux linkages and stator current vectors as state variables, is defined as:

$$
T_e = \frac{3P}{4} \frac{L_m}{L_r} \left(i_{\beta s} \lambda_{\alpha r} - i_{\alpha s} \lambda_{\beta r} \right) . \tag{24}
$$

Once defined the electromagnetic torque, the angular movement equation of the induction motor is defined by:

$$
J_m \frac{d}{dt} \omega_m = \frac{3P}{4} \frac{L_m}{L_r} \left(i_{\beta s} \lambda_{\alpha r} - i_{\alpha s} \lambda_{\beta r} \right) - B_m \omega_m - T_L , \tag{25}
$$

where the term of the left side is defined as the acceleration torque, the second term of the right side is the frictional torque and the last term is the torque established for the mechanical load driven by the motor. After the whole process, the induction motor model is defined combining the state equations of the rotor flux linkages vector (17), stator current vector (19), and rotor angular velocity (25). Then, the mathematical model of squirrel-cage induction

motor on the $\alpha\beta$ coordinated frame is:

$$\frac{d}{dt}\omega_m = K_T\left(i_{\beta s}\lambda_{\alpha r} - i_{\alpha s}\lambda_{\beta r}\right) - \frac{B_m}{J_m}\omega_m - \frac{1}{J_m}T_L$$

$$\frac{d}{dt}\begin{bmatrix} \lambda_{\alpha r} \\ \lambda_{\beta r} \end{bmatrix} = \begin{bmatrix} -\frac{1}{T_r} & -\frac{P}{2}\omega_m \\ \frac{P}{2}\omega_m & -\frac{1}{T_r} \end{bmatrix}\begin{bmatrix} \lambda_{\alpha r} \\ \lambda_{\beta r} \end{bmatrix}$$

$$+ \begin{bmatrix} \frac{L_m}{T_r} & 0 \\ 0 & \frac{L_m}{T_r} \end{bmatrix}\begin{bmatrix} i_{\alpha s} \\ i_{\beta s} \end{bmatrix} \tag{26}$$

$$\frac{d}{dt}\begin{bmatrix} i_{\alpha s} \\ i_{\beta s} \end{bmatrix} = \begin{bmatrix} \frac{\delta}{T_r} & \frac{P}{2}\delta\omega_m \\ -\frac{P}{2}\delta\omega_m & \frac{\delta}{T_r} \end{bmatrix}\begin{bmatrix} \lambda_{\alpha r} \\ \lambda_{\beta r} \end{bmatrix}$$

$$+ \begin{bmatrix} -\gamma & 0 \\ 0 & -\gamma \end{bmatrix}\begin{bmatrix} i_{\alpha s} \\ i_{\beta s} \end{bmatrix} + \begin{bmatrix} \frac{1}{\sigma L_s} & 0 \\ 0 & \frac{1}{\sigma L_s} \end{bmatrix}\begin{bmatrix} v_{\alpha s} \\ v_{\beta s} \end{bmatrix}$$

with the following parameter constants defined as: $K_T = \dfrac{3P}{4}\dfrac{L_m}{J_m L_r}$, $T_r = \dfrac{L_r}{R_r}$, $\delta = \dfrac{1-\sigma}{\sigma L_m}$, $\gamma = \dfrac{1}{\sigma T_s} + \dfrac{1-\sigma}{\sigma T_r}$, $\sigma = 1 - \dfrac{L_m^2}{L_s L_r}$ and $T_s = \dfrac{L_s}{R_s}$. The machine parameters are defined as: R_s is the stator resistance per phase, R_r' is the rotor resistance per phase referred to stator winding, L_s is the stator inductance, which is defined in (11), L_m is the mutual-inductance defined in (12), and L_r is the rotor inductance defined in (15). P is the number of poles, B_m is the friction coefficient of the shaft, and J_m is the inertial moment. T_L is the load torque as mechanical input, $v_{\alpha s}$ and $v_{\beta s}$ are the input voltages that feed the stator winding.

It is important to mention that the procedure to obtain the mathematical model of the induction motor is not new, but the proposed methodology for establishing the mathematical model of the squirrel-cage induction motor is highly detailed, where the rotor inductance, stator inductance and mutual inductance are defined formally when setting the model at $\alpha\beta$ coordinate frame. The proposed methodology can be easy applied for obtaining the mathematical model of any other type of ac machine, such as the doubly-fed induction generator, synchronous machine, and permanent-magnet machine.

2.1   Rotor flux linkages observer

From induction motor model (26) and considering the angular velocity ω_m as a known input, electrical model becomes linear and it is represented by:

$$\frac{d}{dt}\begin{bmatrix} \boldsymbol{\lambda}_r \\ \mathbf{i}_s \end{bmatrix} = \begin{bmatrix} \mathbf{A}_{11} & \mathbf{A}_{12} \\ \mathbf{A}_{21} & \mathbf{A}_{22} \end{bmatrix}\begin{bmatrix} \boldsymbol{\lambda}_r \\ \mathbf{i}_s \end{bmatrix} + \begin{bmatrix} 0 \\ \mathbf{B} \end{bmatrix}\mathbf{v}_s$$

$$y = \begin{bmatrix} 0 & 1 \end{bmatrix}\begin{bmatrix} \boldsymbol{\lambda}_r \\ \mathbf{i}_s \end{bmatrix}.$$

$$(27)$$

where the output variable is defined by the stator current vector $\mathbf{i}_s$, which is the measurement variable. The system (27) can be transformed to new system of reducer order as:

$$\frac{d}{dt}\boldsymbol{\lambda}_r = \mathbf{A}_{11}\boldsymbol{\lambda}_r + \mathbf{A}_{12}\mathbf{i}_s$$

$$\frac{d}{dt}\mathbf{i}_s - \mathbf{A}_{22}\mathbf{i}_s - \mathbf{B}\mathbf{v}_s = \mathbf{A}_{21}\boldsymbol{\lambda}_r$$

$$(28)$$

where the known inputs define the system output. The reduced-order observer model for rotor flux linkages, from model defined in (28), is:

$$\dot{\hat{\boldsymbol{\lambda}}}_r = \mathbf{A}_{11}\hat{\boldsymbol{\lambda}}_r + \mathbf{A}_{12}\mathbf{i}_s + L\left(\frac{d}{dt}\mathbf{i}_s - \mathbf{A}_{22}\mathbf{i}_s - \mathbf{B}\mathbf{v}_s - \mathbf{A}_{21}\hat{\boldsymbol{\lambda}}_r\right),$$

$$(29)$$

where the last term in (29) is a mismatch between the known and observed outputs, and it corrects the system continuously with this error signal.

If the rotor flux observation error variable is defined as:

$$\tilde{\varepsilon}_\lambda = \boldsymbol{\lambda}_r - \hat{\boldsymbol{\lambda}}_r,$$

$$(30)$$

then the observation error dynamics is given by subtracting (29) from (28) to obtain:

$$\dot{\tilde{\varepsilon}}_\lambda = \left(\mathbf{A}_{11} + \mathbf{L}\mathbf{A}_{21}\right)\tilde{\varepsilon},$$

$$(31)$$

where its characteristic equation is defined by:

$$\det\left[s\mathbf{I} - \left(\mathbf{A}_{11} + \mathbf{L}\mathbf{A}_{21}\right)\right] = 0,$$

$$(32)$$

the matrix $\mathbf{L}$ defines the reasonably fast eigenvalues of (31) so that observation error variable decays asymptotically to zero in finite time. These eigenvalues must be at least four or five times faster than the natural eigenvalues of system (28) [13].

By ordering terms in (29), the observer model of the rotor linkages flux takes the form:

$$\dot{\hat{\boldsymbol{\lambda}}}_r = \left(\mathbf{A}_{11} - \mathbf{L}\mathbf{A}_{21}\right)\hat{\boldsymbol{\lambda}}_r + \left(\mathbf{A}_{12} - \mathbf{L}\mathbf{A}_{22}\right)\mathbf{i}_s - \mathbf{L}\mathbf{B}\mathbf{v}_s + \mathbf{L}\frac{d}{dt}\mathbf{i}_s.$$
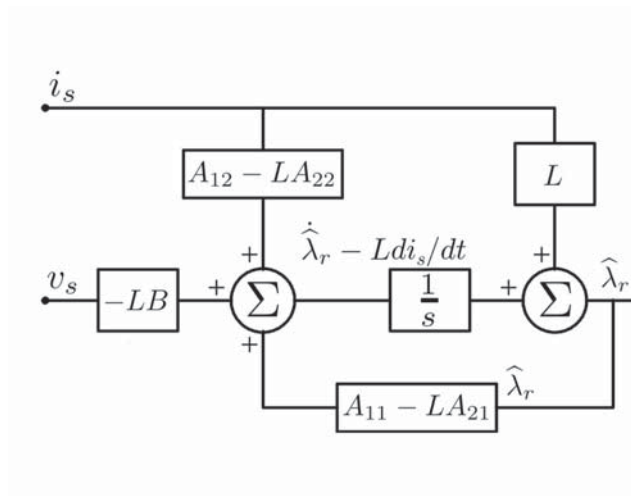
$$(33)$$

If we define

$$\hat{\boldsymbol{\lambda}}_r^* = \hat{\boldsymbol{\lambda}}_r - \mathbf{L}\mathbf{i}_s \,, \tag{34}$$

then the rotor flux linkage observer is defined by:

$$\dot{\hat{\boldsymbol{\lambda}}}_r^* = \left(\mathbf{A}_{11} - \mathbf{L}\mathbf{A}_{21}\right)\hat{\boldsymbol{\lambda}}_r + \left(\mathbf{A}_{12} - \mathbf{L}\mathbf{A}_{22}\right)\mathbf{i}_s - \mathbf{L}\mathbf{B}\mathbf{v}_s, \tag{35}$$

and $\dfrac{d}{dt}\mathbf{i}_s$ no longer appears directly. A block diagram of the reduced-order rotor flux observer is pictured in Fig. 2.

Figure 2. Scheme of the rotor flux linkages observer.

2.2 Load torque observer

Based to induction motor model (26) and by taking the stator current and rotor flux as known inputs, the mechanical model results in:

$$\dot{\omega}_m = K_T \boldsymbol{\lambda}_r^\top \mathbf{M}\mathbf{i}_s - \frac{B_m}{J_m}\omega_m - \frac{1}{J_m}T_L$$

$$\dot{T}_L = 0 \tag{36}$$

A load torque observer can be set as:

$$\dot{\hat{\omega}}_m = K_T \boldsymbol{\lambda}_r^\top \mathbf{M}\mathbf{i}_s - \frac{B_m}{J_m}\hat{\omega}_m - \frac{1}{J_m}\hat{T}_L + l_1\left(\omega_m - \hat{\omega}_m\right)$$

$$\dot{\hat{T}}_L = l_2\left(\omega_m - \hat{\omega}_m\right) \tag{37}$$

If we define the observation error variable to be:

$$\tilde{\varepsilon} = \begin{bmatrix} \omega_m - \hat{\omega}_m \\ T_L - \hat{T}_L \end{bmatrix}. \tag{38}$$

Then the dynamic of this observation error variable is given by subtracting (37) from (36) to get:

$$
\begin{bmatrix} \dot{\tilde{\varepsilon}}_\omega \\[2mm] \dot{\tilde{\varepsilon}}_T \end{bmatrix} = \begin{bmatrix} -\left(\dfrac{B_m}{J_m} + l_1\right) & -\dfrac{1}{J_m} \\[3mm] -l_2 & 0 \end{bmatrix} \begin{bmatrix} \tilde{\varepsilon}_\omega \\[2mm] \tilde{\varepsilon}_T \end{bmatrix}. \tag{39}
$$

where the values of l_1 and l_2 define the reasonably fast eigenvalues of (39), so that the observation error variable is asymptotically steered toward to zero in finite time. These eigenvalues must be at least four or five times faster than the natural eigenvalues of system (36) [13].

3   Induction motor parameter identification

For the purposes of this research, parameter identification of the squirrel-cage induction motor model is made with off-line dynamics and steady-state tests via an acquisition board to determine both electrical and mechanical parameters. The measurement of the dc resistance of the stator winding, no-load test, and blocked-rotor test are applied to induction motor to identify the equivalent circuit model. In addition, we have made the synchronous velocity test to obtain a good approximation of the core loss and calculate the friction loss from the rotational loss. In each one of the tests mentioned, voltage and current measurements of all phases are taken for including any electric unbalance in the stator winding; while, the average power is calculated with very good accuracy by filtering the instantaneous three-phase power. A dynamic test is made when the motor is turned-off and a vector of the velocity fall is captured to obtain an approximate value of the inertial moment J_m using the friction coefficient B_m which is obtained from the consumed power before de-energizing the motor.

3.1   Stator resistance

In this test, ordered pairs consisting of voltage-current measurements are obtained by tuning a DC-voltage source from small to rated current values [12]. The stator winding resistance is calculated applying Ohm's law and assuming star connection of the winding, i.e. we must calculate the resistance as two windings connected in series at $a - b$ terminals, later divide this value by two. The average resistance is obtained from the next set of replications between terminals: $b - c$ and $c - a$, being the result $R_s = 12\ \Omega$.

3.2   No-load test

The no-load test gives information about the magnetizing branch impedance and rotational loss: friction, windage, and core losses, as it is explained in [12]. This test is performed by applying balanced three-phase nominal voltage to the stator winding at the rated frequency. The rotor is kept uncoupled from any shaft of driven equipment.

The equivalent circuit model of the no-load test is depicted in Fig. 3 a), where the branch of the rotor circuit is not considered due to the rotor current is significantly smaller than magnetizing current, due to that in no-load condition the slip is very small and the rotor resistance value is high. The non-load test was carried out at angular velocity of 1798 $r.p.m.$ with a consumed power of 29.04 W. This value was obtained computing and filtering the instant three-phase power to define the average power with very good accuracy. Voltage and current measurements are made in each of the phases to involve any electric imbalance of the stator winding. These measurements are reported in Table 1.

The rotational losses P_{rot} are calculated from the no-load power P_{nl} as follows [12]:

$$P_{rot} = P_{nl} - R_s \left(I_a^2 + I_b^2 + I_c^2 \right) . \tag{40}$$

By substituting the no-load test measurements in (40), the rotational losses are $P_{rot} = 13.5 \ W$.

Base to no-load test, it can be calculated an equivalent reactance composed by the leakage reactance X_{ls}, and magnetizing reactance X_{mag}, see Figure 3 a). For both no-load and blocked rotor tests, the following relationships (41)-(43) are used:

$$|Z_{test}| = \frac{1}{3} \left(\frac{V_a}{I_a} + \frac{V_b}{I_b} + \frac{V_c}{I_c} \right) , \tag{41}$$

$$R_{test} = \frac{P_{test}}{(I_a^2 + I_b^2 + I_c^2)} , \tag{42}$$

$$X_{test} = \sqrt{|Z_{test}^2| - R_{test}^2} . \tag{43}$$

By substituting the measurements of no-load test in (41)-(43), results $Z_{nl} = 182.6 \ \Omega$, $R_{nl} = 22.4 \ \Omega$, and $X_{nl} = 181.2 \ \Omega$.

3.3 Blocked-rotor test

The blocked-rotor test gives information about the leakage impedances and rotor resistance referred to stator side, as it is explained in [12]. In this test the rotor is blocked by a wooden bar so that the motor cannot rotate, and a low voltage is adjusted with a variable supply voltage via a three-phase autotransformer, so that the rated-current flows in stator winding. The power consumption during the test was calculated as 132.4 W. The voltage and current measurements in all phases of this test are reported in Table 2.

As this test is made at low voltage and the slip $s = 1$ due to the rotor is standstill then the rotor resistance is small and the current that flows by the magnetizing branch can be neglected. From the equivalent circuit of this test, see Fig. 3 b), the stator leakage reactance X_{ls} and rotor leakage reactance X'_{lr} are estimated. Additionally, a first approximation of the rotor resistance R_r^* referred to stator side is obtained.

Table 1. Measurements of no-load test.

Stator phase	Voltage (V)	Current (A)
A	119.8	0.67
B	119.8	0.65
C	119.8	0.65

Table 2. Measurements of block-rotor test.

Stator phase	Voltage (V)	Current (A)
a	43.6	1.5
b	43.8	1.5
c	44.7	1.55
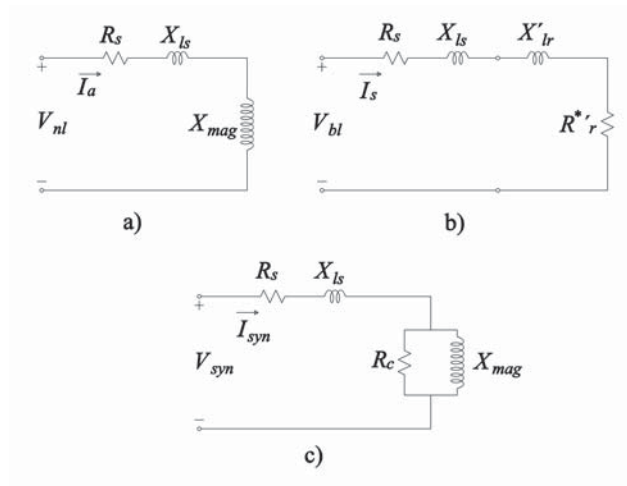
Figure 3. Equivalent circuit of standard tests: a) No-load, b) blocked rotor, and c) Synchronous velocity.

By substituting the blocked-rotor measurements in (41)-(43) we obtain $Z_{bl} = 29.0\ \Omega$, $R_{bl} = 19.2\ \Omega$, $X_{bl} = 21.7\ \Omega$. If one applies the following common approximation to define the stator and rotor leakage reactances, then $X_{ls} = X'_{lr} = \frac{X_{bl}}{2} = 10.8\ \Omega$, where X'_{lr} is referred to stator side by assuming he turns ratio is $a = 1$. Once we know the stator leakage reactance, the magnetizing reactance is calculated from no-load test as $X_{mag} = 170.4\ \Omega$.

From Fig. 3 b), a first approximated value of the rotor resistance referred to stator side can be calculated by:

$$R_r^{*'} = R_{bl} - R_s = 19.2 - 12 = 7.2\ \Omega\ .$$

The rotor resistance value is very important in the induction motor performance because it models largely the power converted from electrical to mechanical energy. Therefore, this value is now improved involving the

magnetizing branch in the equivalent circuit [12]. The new value for rotor resistance is calculated considering the

real part of the Thevenin impedance that is pointed by the arrows in Fig. 4 a), which is:

$$R_r^{*'} = \frac{X_{mag}^2}{R_r'^2 + (X_2' + X_{mag})^2} R_r' . \tag{44}$$
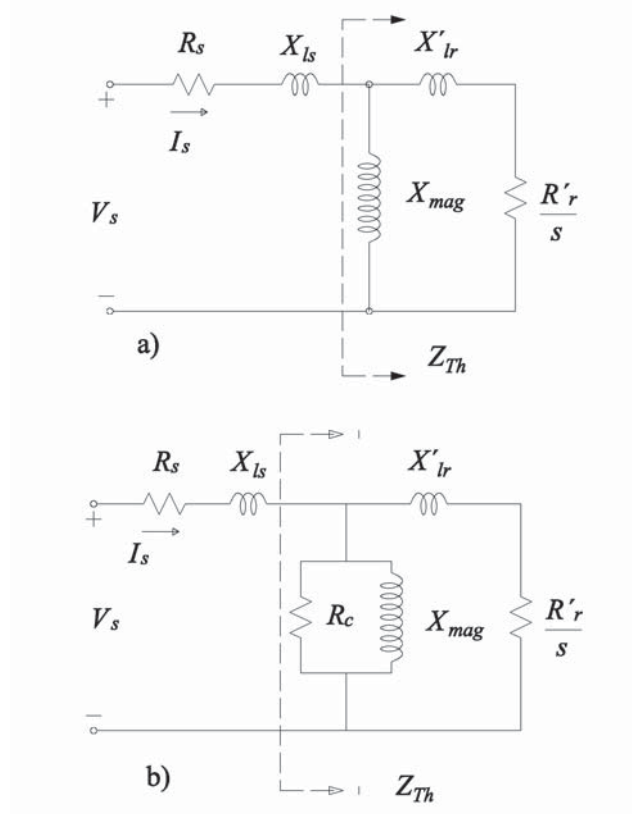
Figure 4. a) Equivalent circuit model and b) Complete equivalent circuit model.

Because $(X_{lr}' + X_{mag})^2 \gg R_r'^2$ in (44), the enhanced value of the rotor resistance is:

$$R_r' = \left(\frac{X_{lr}' + X_{mag}}{X_{mag}}\right)^2 R_r^{*'} , \tag{45}$$

and substituting the values of rotor and magnetizing reactance in (45) yields $R_r' = 8.1\ \Omega$.

3.4   Synchronous velocity test

The synchronous velocity test gives information about the core loss and magnetizing branch impedance with better

accuracy than the no-load test. In this test, a DC-motor drives the induction machine at synchronous velocity and

then the induction machine is feeding at rate voltage. The DC-motor feeds the friction and windage loss for both

machines; while, the power supply feeds the Joule loss and core loss in the induction machine because there are no

induced currents in rotor winding. The equivalent circuit model of the synchronous velocity test is depicted in Fig. 3 c). The consumed power in this test was calculated as 18.1 W. The voltage and current measurements in each of the phases are reported in Table 3.

The core loss P_c is calculated by similar form as rotational loss P_{rot} (40) in no-load test, by:

$$P_c = 18.1 - 12 \left(0.67^2 + 0.65^2 + 0.66^2\right) = 2.4 \, W.$$

3.5 *Mechanical parameters*

The inertial moment J_m and frictional coefficient B_m are the mechanical parameters which model the shaft masses and friction in the support points, respectively; these parameters are involved in the movement equation (25). Due to the squirrel-cage induction motor is mechanically coupled with a dynamometer with which it is possible to vary the load conditions then, the masses and support points of both machines should be considered in the definition of the mechanical parameters. In order to determine the frictional coefficient B_m, the squirrel-cage induction motor is fed at rated voltage without applying load torque. In this test the consumed power was 87.3 W at 1778 $r.p.m.$. The voltage and rotor measurements in all phases of this test are reported in Table 4.

Table 3. Measurements of synchronous test.

Stator phase	Voltage (V)	Current (A)
A	119.9	0.67
B	120.0	0.65
C	120.6	0.66

Table 4. Measurements of coupling no-load test.

Stator phase	Voltage (V)	Current (A)
a	119.8	0.70
b	119.9	0.69
c	120.6	0.72

The rotational loss in both machines applying equation (40), is $P_{rot} = 69.5 \, W$, while the friction loss is the rotational loss (69.5 W) minus core loss (2.4 W), calculated in the synchronous test; then, the friction loss is

$P_{fric} = 67.1\ W$. Consequently, from the mechanical power consumed in this test, the friction coefficient B_m can be approximated as:

$$B_m \approx \frac{P_{fric}}{\omega_m^2} = \frac{67.1}{186.2^2} = 0.00194\ N\ m\ s. \tag{46}$$

From this same test, the inertial moment J_m can be obtained when the induction motor is turned off and a falling velocity vector (see Fig. 5) is captured with an acquisition board. Once the motor is de-energized and it does not drive any mechanical load, the movement equation (25) takes the following form:

$$J_m \frac{d}{dt}\omega_m = -B_m\omega_m. \tag{47}$$

Based on Fig. 5, can be seen the non-filtered and filtered signals of the angular velocity fall when the motor is turned off and the motor shaft stops in 5 seconds, approximately. In this figure, note that two points (2.78 s, 110.7 rad/s) and (3.12 s, 90.33 rad/s) can be used for linearizing the motor's deceleration around the base velocity $\omega_{m0} = 100\ rad/s$; by approximating the derivative at this point, and solving for J_m into (47), the inertial moment can be approximated by:

$$J_m \approx \frac{\Delta t}{\Delta \omega_m} B_m \omega_{m0} \approx \frac{(3.12 - 2.78)}{(110.7 - 90.33)}(0.00194)(100)$$

$$= 0.00324\ N\ m\ s^2. \tag{48}$$
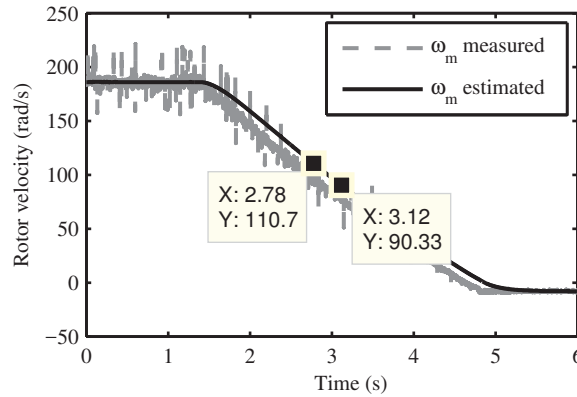
Figure 5. Supply disconnection of the induction motor.

It is important to remark, that the electrical and mechanical parameter identification is made via a data acquisition board, and the voltages and currents are measured in all phases, in contrast to the traditional method where the voltage and current measurements are made in only one phase. Moreover, the consumed power in each one test is computed with accuracy by filtering the instantaneous power, in contrast with traditional method where is

used a wattmeter to measure the consumed power in only one phase. In addition, the synchronous test was made to quantify the core loss which is subtracted from the rotational loss, obtained in no-load test, for estimating the friction coefficient with acceptable accuracy. From the no-load test, the motor is turn-off and a falling velocity vector is captured with an acquisition board for approximating the velocity derivative for estimating the inertial moment value. The proposed procedure to obtain the mechanical parameters contrasts with the work reported in [8], where the two parameters are calculated via the equation movement from the electromagnetic torque which is estimated through rotor resistance whose value is sensitive to temperature changes.

3.6 Relationships between magnetically-coupled circuit and equivalent circuit

It is important to note that the inductance parameters used in the induction motor model (26) correspond to the magnetically-coupled circuit model with the stator-inductance L_s, mutual-inductance L_m, and rotor-inductance L_r which are defined in (11), (12), and (15), respectively; while the inductance parameters obtained from the standard tests which define the equivalent circuit model are the stator leakage inductance X_{ls}, magnetizing inductance X_{mag}, and rotor leakage inductance X'_{lr}. Therefore it is necessary to define the equivalence relationships between the magnetically-coupled circuit and equivalent circuit. At the first step, the voltage equations for two magnetically-coupled circuits are defined as:

$$
\begin{aligned}
v_1 &= L_{11}\frac{d}{dt}i_1 + L_{12}\frac{d}{dt}i_2, \\
v_2 &= L_{12}\frac{d}{dt}i_1 + L_{22}\frac{d}{dt}i_2
\end{aligned}
\tag{49}
$$

where L_{11} and L_{22} are the self-inductances of the primary and secondary windings, respectively; and L_{12} is the mutual-inductance between primary and secondary windings. Thereafter, including the turns ratio $a = N1/N2$ in diverse terms of system (49), keeping the original system, yields:

$$
\begin{aligned}
v_1 &= L_{11}\frac{d}{dt}i_1 + aL_{12}\frac{d}{dt}\frac{i_2}{a} \\
av_2 &= aL_{12}\frac{d}{dt}i_s + a^2 L_{22}\frac{d}{dt}\frac{i_2}{a}
\end{aligned}
\tag{50}
$$

Later, adding and subtracting a different term in each equation of (50) yields:

$$
\begin{aligned}
v_1 &= L_{11}\frac{d}{dt}i_1 + aL_{12}\frac{d}{dt}\frac{i_2}{a} + \left(aL_{12}\frac{d}{dt}i_1 - aL_{12}\frac{d}{dt}i_1 \right) \\
av_2 &= aL_{12}\frac{d}{dt}i_s + a^2 L_{22}\frac{d}{dt}\frac{i_2}{a} + \left(aL_{12}\frac{d}{dt}\frac{i_2}{a} - aL_{12}\frac{d}{dt}\frac{i_2}{a} \right)
\end{aligned}
\tag{51}
$$

Finally, rearranging terms in (51), we obtain a model that correspond to the equivalent circuit model, which is shown in Figure 6, and this model takes the form:

$$
\begin{aligned}
v_1 &= (L_{11} - aL_{12})\frac{d}{dt}i_1 + aL_{12}\left(\frac{d}{dt}i_1 + \frac{d}{dt}\frac{i_2}{a} \right) \\
av_2 &= aL_{12}\left(\frac{d}{dt}i_1 + \frac{d}{dt}\frac{i_2}{a} \right) + (a^2 L_{22} - aL_{12})\frac{d}{dt}\frac{i_2}{a}
\end{aligned}
\tag{52}
$$
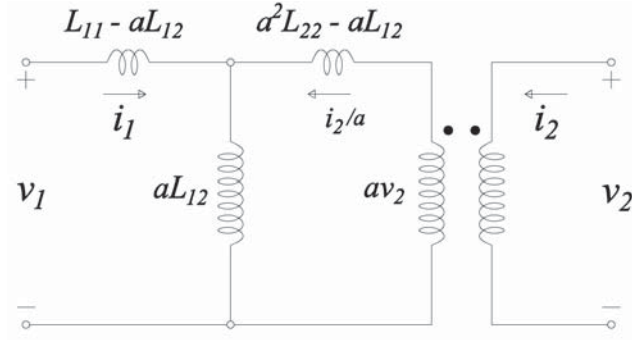
Figure 6. Equivalence between magnetically-coupled and equivalent circuits.

Now, comparing Figures 4 a) and 6, without considering the resistances, we can set the relationships that define the inductance equivalence between the magnetically-coupled circuit and the equivalent circuit of the following form:

$$L_{ls} = L_{11} - aL_{12}, \tag{53}$$

$$L_{mag} = aL_{12}, \tag{54}$$

$$L'_{lr} = a^2 L_{22} - aL_{12} . \tag{55}$$

It is common practice to consider the ratio turns $a = 1$ for the squirrel-cage induction motor. From (12) and (54), the relationship between the mutual-inductance L_m, which is used in the induction motor model (26), and magnetizing inductance L_{mag} results in:

$$L_m = \frac{3}{2} L_{mag} . \tag{56}$$

From (53) and (11), and considering that the mutual-inductance between two stator phases is $L_{sm} = -\frac{1}{2} L_{mag}$ [11], we obtain the stator inductance which is used in the model (26) as:

$$L_s = L_{ls} + \frac{3}{2} L_{mag} . \tag{57}$$

With a same procedure, the rotor inductance used in model (26) is defined as:

$$L_r = L'_{lr} + \frac{3}{2} L_{mag} . \tag{58}$$

By applying (56), (57), and (58) the equivalence between magnetically-coupled model and equivalent circuit model is defined. In Table 5, values obtained from parameter identification process for induction motor model (26) have been sumarized. In Table 6, squirrel-cage induction motor nameplate data (rated values) are reported.

Table 5. Induction motor model parameters.

Parameter	Value
R_s	12 Ω
R_r	8.1 Ω
L_s	0.7066 H
L_r	0.7066 H
L_m	0.678 H
B_m	0.00194 $N\ m\ s$
J_m	0.00324 $N\ m\ s^2$

Table 6. Induction motor nameplate data.

Unit	Value
Volts	127/220
Amperes	1.5
$r.p.m.$	1750
Hz	60
HP	0.25

So far we have obtained the electric parameters of the equivalent circuit (Fig. 4 a). Now, we propose a complete equivalent circuit just in order to obtain a comparative analysis between both models. The complete equivalent circuit involves the core loss represented with a resistor R_c (Fig. 4 b) and the values of the magnetizing reactance X_{mag}, rotor leakage reactance X'_{lr}, and rotor resistance R'_r are more accurate due to the fact that now the analysis is made from synchronous velocity test and blocked-rotor tests. This is achieved by considering the Thevenin impedance pointed in Fig. 4 b). By applying equations (41), (42) and (43) to data obtained from synchronous test in Table 3, results $R_{syn} = 13.85\ \Omega$ and $X_{syn} = 181.57\ \Omega$, and solving the following non-linear system set from Fig. 3 c):

$$
\begin{aligned}
R_{syn} &= R_s + \frac{R_c X_{mag}^2}{R_c^2 + X_{mag}^2} \\
X_{syn} &= X_{ls} + \frac{R_c X_{mag}^2}{R_c^2 + X_{mag}^2}
\end{aligned}, \tag{59}
$$

where $R_s = 12\ \Omega$, $X_{ls} = 10.8\ \Omega$ and the parameters R_c and X_{mag} are unknown. The results obtained from (59) are: the core loss $R_c = 15,765\ \Omega$, and magnetizing reactance $X_{mag} = 170.8\ \Omega$. In a similar form, by considering the results from blocked-rotor test $R_{bl} = 19.2\ \Omega$ and $X_{bl} = 21.7\ \Omega$, defining $K_1 = \frac{R_c X_{mag}}{R_c^2 + X_{mag}^2}$, and solving the

following non-linear system from Fig. 4 b) for unknown parameters R'_r and X'_{lr}:

$$R_{bl} = R_s + K_1 \frac{AB + CD}{E}$$

$$X_{bl} = X_{ls} + K_1 \frac{CB - AD}{E}$$

(60)

where $A = R'_r X_{mag} - R_c X'_{lr}$, $B = K_1 X_{mag} + R'_r$, $C = R_c R'_r + X'_{lr} X_{mag}$, $D = K_1 R_c + X'_{lr}$, and $E = (K_1 X_{mag} + R'_r)^2 + (K_1 R_c + X'_{lr})^2$.

The results obtained from (60) are: rotor resistance $R'_r = 8.2 \ \Omega$ and rotor leakage reactance $X'_{lr} = 11.3 \ \Omega$. It is important to remark that the electric parameters of the complete equivalent circuit model are very close to parameters obtained from the no-load and blocked-rotor tests; consequently, the approximations made in these tests are justified. In Table 7 can be seen the minimum differences between the parameter values of the magnetizing and rotor branches

**Table 7.** Magnetizing and rotor branches parameters.

Parameter	Equivalent circuit (Ω)	Complete equivalent circuit (Ω)
R_c	∞	15,765
X_{mag}	170.4	170.8
R'_r	8.1	8.2
X'_{lr}	10.8	11.3

4 Induction motor model, observers and parameter identification validation

Experimental validation was made using the following devices:

- A squirrel-cage induction motor (Lab-Volt 8221-02) coupled via belt with a dynamometer (Lab-Volt 8960-12) with velocity sensor, see Fig. 7.

- dSPACE DS1103 data acquisition board with real-time interface (RTI) to display signals.

- A measurement interface for currents in each phase and two line-to-line voltages in stator terminals.

In order to validate the mathematical model (26), rotor flux linkages observer (35), load torque observer (37), and the parameter identification, the squirrel-cage induction motor is operated under variable load conditions, where the load torque is applied by a dynamometer. An array with 10 s length and 100 μs sampling time was captured for electrical and mechanical signals. Then, the similitude transformation was applied in real time to stator voltages v_{ab}, v_{cb} and stator currents i_a, i_b, and i_c to refer them at $\alpha - \beta$ coordinated frame. The angular velocity ω_m and
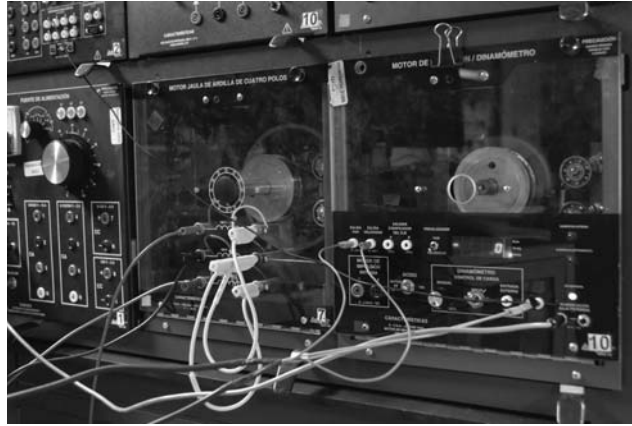
Figure 7. Induction motor-dynamometer group.

stator currents $i_{\alpha s}$ (phase-a) are compared graphically between their measured values and corresponding results obtained via simulation. It is important to remark that the mathematical model (26) and rotor flux linkages observer (35) are validated by means of the comparison between the measured load torque with the observed load torque (37). With this, the mechanical oscillation equation (25) is fulfilled where stands out the electromagnetic torque (24), as nonlinear term, which involves a sum of two electrical state space variables products of system (26).

The induction motor as electromechanical device has two inputs: the stator voltages and the load torque. In the first test, the motor is subjected to step response by applying the nominal voltage at stator winding and the motor is turned-on. In the second test, the load torque is changed from no-load condition to nominal operation condition in five successive steps establishing different points of operation of the motor. In Fig. 8 the induction motor starts on under no-load condition is shown, the rotor velocity simulated and measured are very close when the velocity arise, without the use of a filter to avoid a delay in velocity measurement. By turning a potentiometer in DC-machine module, five load torque levels were set up, from no-load to rated condition, where the rated torque is $T_L = 1\,N\,m$. In Fig. 9 a), rotor angular velocity ω_m measured by encoder and rotor velocity obtained via simulation of proposed model (26) are displayed. Note that in this figure, there are two indicated values at 5.0 s time, which are 1746 and 1740 $r.p.m.$, measured and simulated velocities, respectively; and the difference between both velocities is minimal of 6 $r.p.m.$ with a relative error of 0.3 %. In Fig. 9 b), the variations of load torque measured and load torque estimated via an asymptotic observer are depicted, where there is not difference. In Fig. 10 a), the stator current at α-axis, which corresponds with the phase-a of three-phase system is shown. When the load torque is changed, then the stator currents change, too. The stator current $i_{\alpha s}$ does not present good approximation between the measured (1.25 A rms) and simulated signal (0.95 A rms), as shown in Fig. 10 b). The difference between

the stator current simulated and measured is notorious due to core loss are not involved in parameter identification process.

It is important remark that all state variables are involved into movement equation; therefore, as the observed load torque is very close to the measured load torque then the mathematical model and its parameter identification is validated.
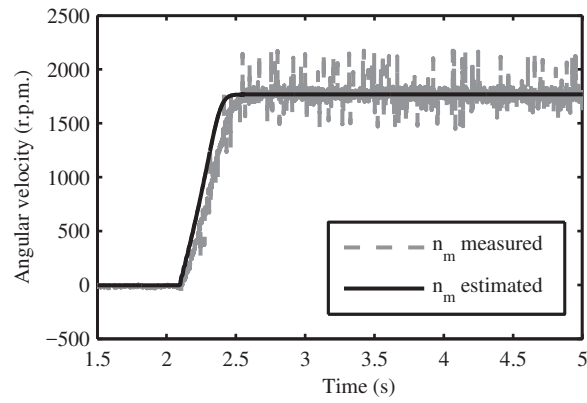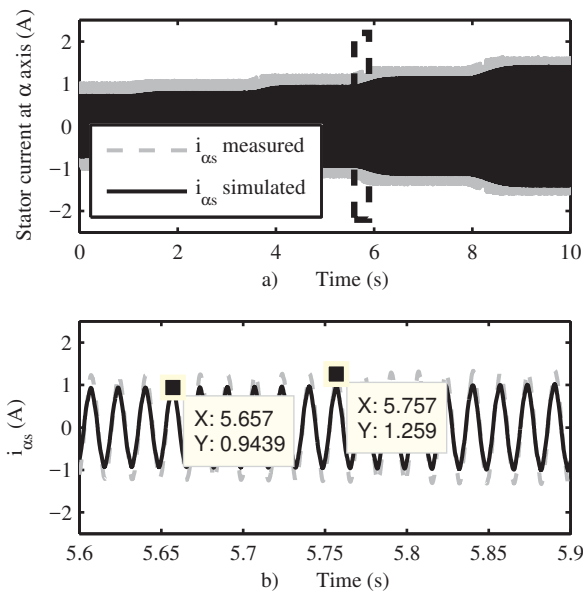

Figure 8. Starting of induction motor.
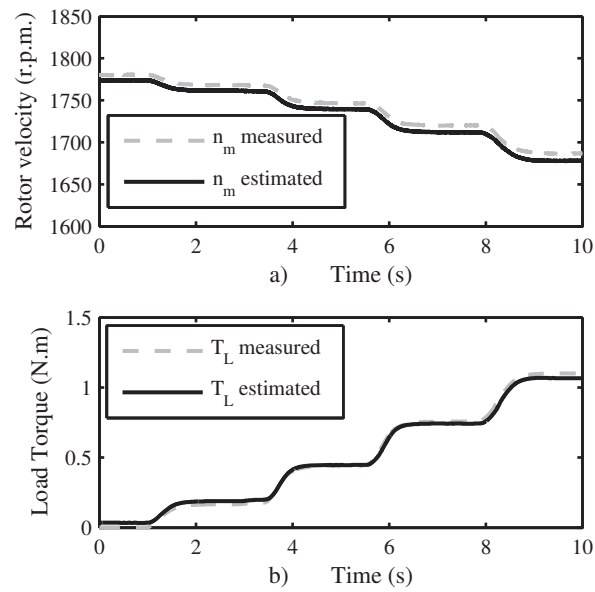
Figure 9. Mechanical variables a) Rotor angular velocity, and b) Load torque.

Figure 10. a) Stator current $i_{\alpha s}$ (phase-a), b) detail of stator current at α-axis.

5   Conclusions

On this paper, a step-by-step procedure is presented to obtain the mathematical model of the squirrel-cage induction

motor at $\alpha\beta$ coordinate frame. In order to carry out the electric parameter identification procedure, no-load test

and blocked-rotor test were applied in steady state to obtain the equivalent circuit model of the induction motor.

In addition, the synchronous velocity test was made to approximate the core loss which is included in the results

obtained at no-load test where the induction motor is coupled to a dynamometer via a belt. From this test, the friction

coefficient B_m is approximated from the mechanical power developed at the shaft which is calculated separating

the core loss from rotational loss; later, the inertial moment J_m is estimated from movement equation when the

motor is de-energized by capturing velocity as it falls and approximating its derivative. In addition, we propose the

equivalence relationships for changing the inductance parameters from equivalent circuit model to magnetically-

coupled circuit model. The equivalent circuit model is used to predict the steady state performance of the induction

motor, meanwhile the mathematical model in $\alpha\beta$ frame has parameters of the magnetically-coupled circuit model.

Finally, in order to validate the mathematical model and its parameter identification was made a steady state test

where the load conditions are varied by a dynamometer. We can clearly see on the obtained signal plots, a very

close similarity between simulation and measured signals of the induction motor. It is important to remark that the

mathematical model of the induction motor, the state observer models and the parameter identification constitutes

an important aspect in the designing of robust closed-loop controllers with high performance.

Acknowledgment

References

[1] L. Peretti and M. Zigliotto, Automatic procedure for induction motor parameter estimation at standstill, *IET Electric Power Applications*, vol. 6, no. 4, pp. 214–224, 2012.

[2] M. Carraro and M. Zigliotto, Automatic parameter identification of inverter-fed induction motors at standstill, *IEEE Transactions on Industrial Electronics*, vol. 61, no. 9, pp. 4605–4613, 2014.

[3] H. Yanhui. W. Yue, F. Yupeng, and W. Zhaoan, Parameter Identification of an Induction Machine at Standstill Using the Vector Constructing Method, *IEEE Transactions on Power Electronics*, vol. 27, no. 2, pp. 905–915, 2012.

[4] E. Laroche and M. Boutayeb, Identification of the induction motor in sinusoidal mode, *IEEE Transactions on Energy Conversion*, vol. 25, no. 1, pp. 11–19, 2010.

[5] Y. Koubaa, Recursive identification of induction motor parameters, *Simulation Modelling Practice and Theory*, vol. 12, no. 5, pp. 363–381, 2004.

[6] F. Duan, R. Zivanovic, S. Al-Sarawi and D. Mba, Induction motor parameter estimation using sparce frid optimization algorithm, *IEEE Transactions on Industrial Informatics*, vol. 12, no. 4, pp. 1453–1461, 2016.

[7] P. Kumar, A. Dalal, and A. K. Singh, Identification of three phase induction machines equivalent circuits parameters using multi-objective genetic algorithms, *IEEE International Conference on Electrical Machines (ICEM 2014)*, pp. 1211–1217, 2014.

[8] L. Whei-Min, S. Tzu-Jung, and W. Rong-Ching, Parameter identification of induction machine with a starting no-load low-voltage test, *IEEE Transactions on Industrial Electronics*, vol. 58, no. 1, pp. 352–359, 2012.

[9] C. Laughman, S. B. Leeb, L. K. Norford, S. R. Shaw and P. R. Armstrong, A two-step method for estimating the parameters of induction machine models, *Energy Conversion Congress and Exposition, ECCE 2009*, pp. 262-269, 2009.

[10] Song Wang, V. Dinavahi, and Jian Xiao, Multi-rate real-time model-based parameter estimation and state identification for induction motors, *IET Electric Power Applications*, vol. 7, no. 1, pp. 77–86, 2013.

[11] P. Krause, O. Wasynczuk and S. Sudhoff, Analysis of Electric Machinery and Drive Systems, New York: IEEE Press Power Engineering, 2002.

[12] P. C. Sen, Principles of Electric Machines and Power Electronics. Kingstone, Ontario: John Wiley and Sons, 1997.

[13] G. N. Franklin , J. D. Powell and A. Emami-Naeini, Feedback Control of Dynamics Systems, New Jersey: Prentice Hall, 2002